

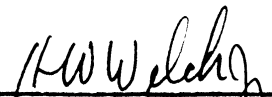
ENGINEERING RESEARCH INSTITUTE
UNIVERSITY OF MICHIGAN
ANN ARBOR

A TOROIDAL SAMPLE HOLDER FOR MEASURING VHF PERMEABILITY AND LOSSES

Technical Report No. 35
Electronic Defense Group
Department of Electrical Engineering

By: Paul E. Nace

Approved by:


H. W. Welch, Jr.


D. M. Grimes

Project 2262

TASK ORDER NO. EDG-6
CONTRACT NO. DA-36-039 sc -63203
SIGNAL CORPS, DEPARTMENT OF THE ARMY
DEPARTMENT OF ARMY PROJECT NO. 3-99-04-042
SIGNAL CORPS PROJECT NO. 194B

July, 1954

TABLE OF CONTENTS

| | Page |
|---|------|
| LIST OF ILLUSTRATIONS | iii |
| ABSTRACT | iv |
| 1. INTRODUCTION | 1 |
| 2. MATHEMATICAL ANALYSIS | 1 |
| 2.1 Section One | 1 |
| 2.2 Section Two | 5 |
| 2.3 Section Three | 7 |
| 2.4 Wall Losses and Internal Inductance | 7 |
| 2.5 Accuracy | 8 |
| 3. DESIGN | 9 |
| 4. MEASUREMENTS | 10 |
| 4.1 Impedance Measuring Apparatus | 10 |
| 4.2 Measurements with the Three Coaxial Inductors | 11 |
| 4.3 Calibration | 11 |
| 4.4 The Value of Characteristic Impedance, Z_0 | 18 |
| 4.5 Procedure | 18 |
| 4.6 Z- θ Chart | 21 |
| 4.7 P-Contours | 21 |
| 5. CONCLUSION | 24 |
| ACKNOWLEDGEMENTS | 24 |

LIST OF ILLUSTRATIONS

| | Page |
|---|------|
| Figure 1 Coaxial Inductor No. 1 | 2 |
| Figure 2 Coaxial Inductor No. 2 | 3 |
| Figure 3 Assembly, Coaxial Inductor No. 3 | 12 |
| Figure 4 μ_1 and μ_2 Measured by Different Inductors | 13 |
| Figure 5 μ_1 and μ_2 Measured by Different Inductors | 14 |
| Figure 6 Calibration Curves: $l_2 + l_3$ vs $\frac{\omega}{2\pi}$ | 15 |
| Figure 7 Calibration Curves: $\frac{Z_a}{\omega/\omega_0}$ vs $\frac{\omega}{2\pi}$ | 17 |
| Figure 8 Sections II and III of Coaxial Inductor No. 2: The Transmission Line | 19 |
| Figure 9 μ -Curves Using Two Different Values of Z_0 | 20 |
| Figure 10 P-Contours | 23 |

ABSTRACT

A toroidal sample holder suitable for measuring the permeability and magnetic losses of ferrite toroids is described. Equations describing its operation are derived and design problems are discussed. The approximations used and the sources of error are evaluated. Calibration curves are presented. A graphical means of determining the permeability and losses of the ferrite from the measured value of impedance is described. The sample holder has been used over a frequency range of 30 Mc/s to 500 Mc/s.

A TOROIDAL SAMPLE HOLDER FOR MEASURING VHF PERMEABILITY AND LOSSES

1. INTRODUCTION

The coaxial inductor is a toroidal sample holder suitable for use at "very high frequencies" for the measurement of the permeability and the magnetic losses of a ferrite ring independent of associated circuit parameters. Used with suitable impedance measuring apparatus it allows rapid measurements on large numbers of cores.

The coaxial inductor is composed of three sections: 1. A one-turn toroidal inductance which takes the form of a short length of coaxial line terminated in a short circuit; 2. A taper section which transforms the inner and outer radii of section 1 to the radii of a standard coaxial transmission line; 3. A coaxial transmission line joining section 2 to the point at which an impedance measurement can be made. Figure 1 shows a coaxial inductor which was used at the University of Michigan. Figure 2 shows an improved design which is currently in use. The three sections of the inductor are considered separately in the mathematical analysis which follows.

2. MATHEMATICAL ANALYSIS

2.1 Section One

A length of transmission line which is much shorter than a radian in electrical length may be treated as a lumped impedance. A longer length must be treated as a distributed impedance. The impedance Z_A of a shorted section of line of length l_1 and inner and outer radii of r_i and r_o is:¹

¹ Ramo, S. and Whinnery, J. R., Fields and Waves in Modern Radio, John Wiley and Sons, New York, 1944, p. 47

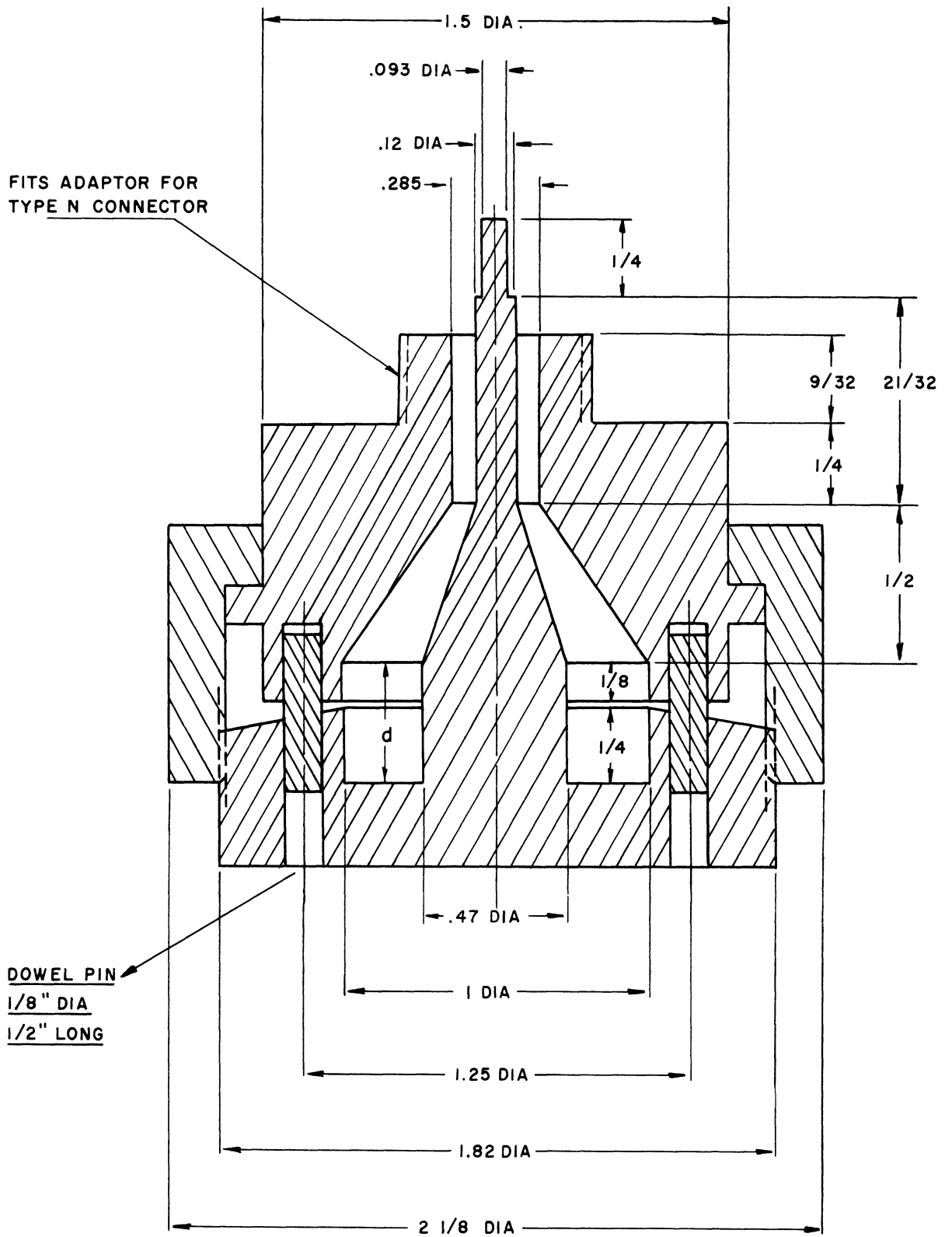


FIG. 1

COAXIAL INDUCTOR NO 1

DIMENSION IN INCHES

SCALE 2x

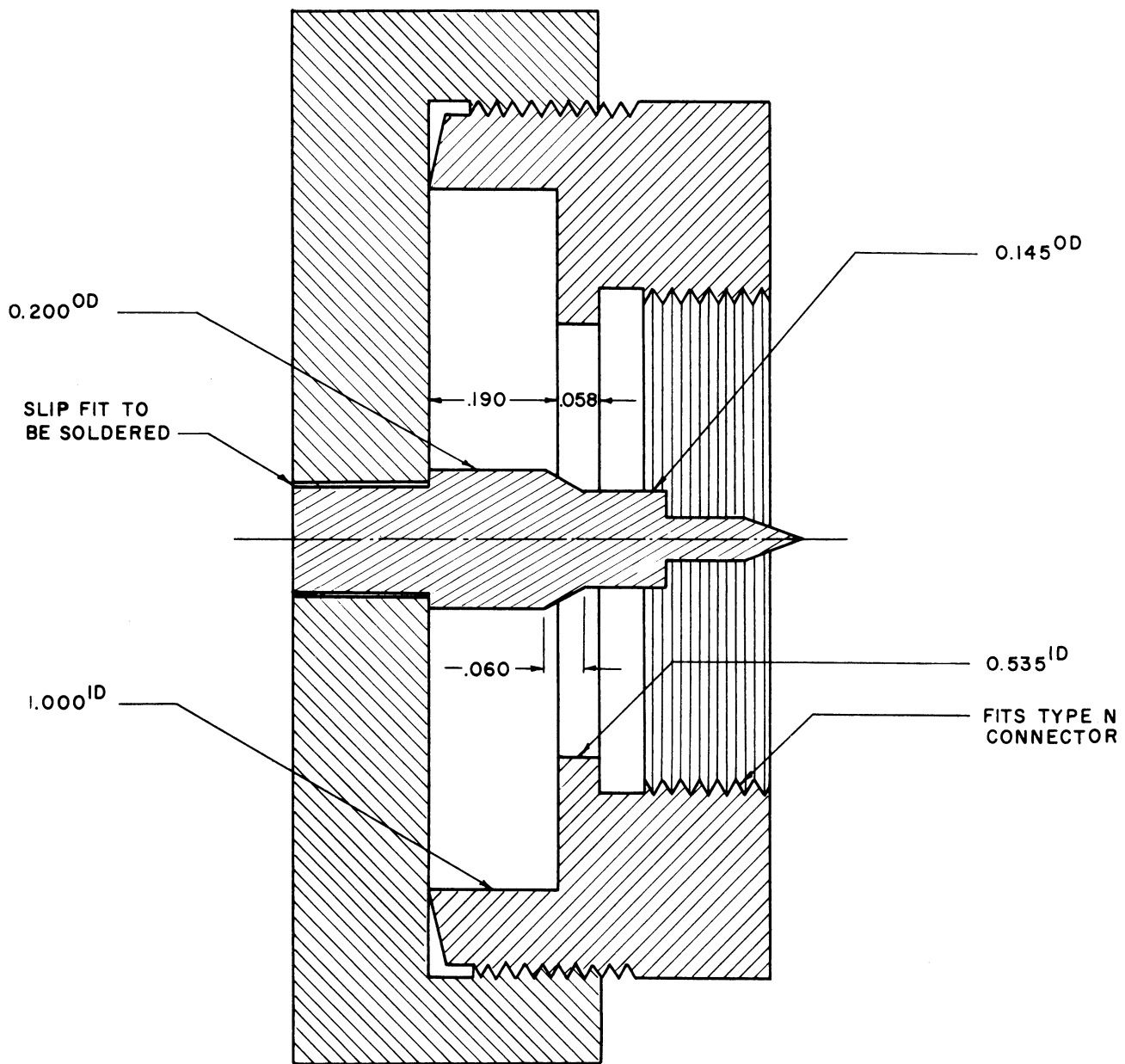


FIG 2

COAXIAL INDUCTOR NO 2

DIMENSIONS IN INCHES SCALE 4x

$$Z_A = Z_0 \tanh \gamma \ell_1 \cong Z_0 \gamma \ell_1 \text{ for } \ell_1 \ll \frac{\lambda}{4}, \text{ i.e., for } |\gamma \ell_1| < 0.1. \quad (1)$$

where² $\gamma = \alpha + j\beta = j\omega\sqrt{\mu\epsilon}$ = propagation constant

and² $Z_0 = \frac{1}{2\pi} \sqrt{\frac{\mu}{\epsilon}} \log_e \frac{r_o}{r_i}$ = characteristic impedance.

μ and ϵ are the permeability and dielectric constant of the dielectric medium.

$$Z_A = j \frac{\omega\mu\ell_1}{2\pi} \log_e \frac{r_o}{r_i} = j\omega L_A \quad (2)$$

Here L_A is the inductance of section one. Since $\mu = \mu_o = \frac{4\pi}{10^7}$ hy/m for the air dielectric, there are no dielectric losses. That wall losses and internal inductance are negligible will be established later.

This short length of shorted line is equivalent to a one-turn toroid and we shall show this latter approach leads to the same equation. But first consider a one-turn toroid with a two-media core, a ferromagnetic ring that partly fills the region plus air that fills the remainder of the region within the single turn. We require the ferromagnetic ring to be positioned concentrically and to have the dimensions r_1 and r_2 for inner and outer radii and ℓ_f for axial length. It has a permeability of $\mu = (\mu_1 - j\mu_2) \mu_o$

$$H = \frac{i}{2\pi r} \quad (\text{amps/m})$$

The flux through the area A , the cross-section of the toroid, is:

$$\phi = \int_A \bar{B} \cdot d\bar{A} \quad \text{webers} \quad (3)$$

² Ibid, p. 332

Taking the integral in two parts — over the entire region with the air permeability μ_0 and over the ferromagnetic region with the contribution to ϕ over and above what an air medium would contribute — gives:

$$\begin{aligned} \phi &= \int_{r_i}^{r_o} \mu_0 H \ell_1 dr + \int_{r_i}^{r_2} (\mu - \mu_0) H \ell_f dr \\ &= \frac{j\mu_0}{2\pi} \left[\ell_1 \log_e \frac{r_o}{r_i} + \frac{\mu - \mu_0}{\mu_0} \ell_f \log_e \frac{r_2}{r_i} \right] \end{aligned} \quad (4)$$

$$Z_1 = j\omega L_1 = j\omega \frac{d\phi}{di} = j \frac{\omega\mu_0}{2\pi} \left\{ \ell_1 \log_e \frac{r_o}{r_i} + \ell_f \left[\frac{\mu}{\mu_0} - 1 \right] \log_e \frac{r_2}{r_i} \right\} \quad (5)$$

If the ferromagnetic ring is removed, i.e., $\ell_f = 0$, Eq 5 becomes identical with Eq 2 as predicted above.

2.2 Section Two

If the taper section is short enough or if the change in $\frac{r_o}{r_i}$ is small from the input to the output of the section, we can treat it as a transmission line section with a constant characteristic impedance. Otherwise one must calculate the impedance transfer function of this taper section.

Consider a linear taper of length l_2 and with radii:

$$r_o = k_o(x + x_o) \text{ and } r_i = k_i(x + x_i)$$

$$\frac{r_o}{r_i} = k \frac{x + x_o}{x + x_i} \quad \text{where } k = \frac{k_o}{k_i}$$

Let us require $l_1 + l_2 \ll \lambda$. Then lumped-circuit techniques can be used.

We treat the section as a single-turn toroid.

$$\begin{aligned}
 L_T &= \frac{d\phi}{di} = \frac{1}{i} \int_A \vec{B} \cdot d\vec{A} = \frac{1}{i} \int_0^{\ell_2} \int_{r_i}^{r_o} \mu_o H dr dx \\
 &= \frac{\mu_o}{2\pi} \int_0^{\ell_2} \log_e \left(k \frac{x + x_o}{x + x_i} \right) dx
 \end{aligned} \tag{6}$$

$$= \frac{\mu_o k (x_i - x_o)}{2\pi} \left[\int \frac{\log_e y dy}{(y-k)^2} \right]_{k \frac{x_o}{x_i}}^{k \frac{\ell_2 + x_o}{\ell_2 + x_i}}$$

where $y = k \frac{x + x_o}{x + x_i}$ and $H = \frac{i}{2\pi r}$

Integrating by parts:

$$\begin{aligned}
 L_T &= \frac{\mu_o k}{2\pi} (x_i - x_o) \left[\frac{-\log_e y}{y-k} + \int \frac{dy}{y(y-k)} \right]_{k \frac{x_o}{x_i}}^{k \frac{\ell_2 + x_o}{\ell_2 + x_i}} \\
 &= \frac{\mu_o k}{2\pi} (x_i - x_o) \left[\frac{-\log_e y}{y-k} + \frac{\log_e(y-k)}{k} - \frac{\log_e y}{k} \right]_{k \frac{x_o}{x_i}}^{k \frac{\ell_2 + x_o}{\ell_2 + x_i}} \\
 &= \frac{\mu_o}{2\pi} \left\{ \ell_2 \log_e k \frac{x_o}{x_i} + \ell_2 \log_e \left[\frac{x_i}{x_o} \cdot \frac{\ell_2 + x_o}{\ell_2 + x_i} \right] + \right. \\
 &\quad \left. + x_i \log_e \frac{x_i}{\ell_2 + x_i} - x_o \log_e \frac{x_o}{\ell_2 + x_o} \right\}
 \end{aligned} \tag{7}$$

If $x_o = x_i$ in Eq 7 it becomes Eq 2. The error introduced by treating the taper as a constant impedance transmission line is given by the last three terms in Eq 7. If this error is small enough the taper section can be treated as a constant impedance transmission line. If we do this we introduce an error by neglecting the taper, but counteract the error introduced in calculating Eq 7, namely, using lumped circuit methods. This will become apparent in the next section.

2.3 Section Three

The impedance Z_3 at the input of a transmission line of length l_3 terminated in an impedance Z_2 is:³

$$Z_3 = Z_0 \frac{Z_2 \cosh \gamma l_3 + Z_0 \sinh \gamma l_3}{Z_0 \cosh \gamma l_3 + Z_2 \sinh \gamma l_3} \quad (8)$$

$$\cong Z_0 \frac{Z_2 + jZ_0 \tan \beta l_3}{Z_0 + jZ_2 \tan \beta l_3} \quad \text{for a low loss line} \quad (9)$$

This equation treats the transmission line as a distributed impedance. If it is sufficiently accurate to treat the taper as a constant impedance transmission line, Z_1 can be substituted for Z_2 and $l_2 + l_3$ for l_3 in Eq 9. In this way the error introduced by the lumped circuit approximation is avoided.

2.4 Wall Losses and Internal Inductance

These are negligible since the wall impedance is negligibly small compared to the impedances calculated above. The depth of penetration is:⁴

$$\delta = \left[\frac{2}{\omega \mu_0 \sigma_w} \right]^{1/2} \quad \text{meters} \quad (10)$$

where σ_w = wall conductivity.

The wall impedance Z_w is:⁵

$$Z_w = \frac{1 + j}{2 \pi \delta \sigma_w} \left(\frac{1}{r_0} + \frac{1}{r_1} \right) = R + j\omega L_w \quad \text{ohms/meter} \quad (11)$$

³ Reference Data for Radio Engineers, 3rd Edition, Federal Telephone and Radio Corporation, 1949, p. 311

⁴ Page 204 of Ramo and Whinnery, op.cit.

⁵ Pages 332-333 of Ramo and Whinnery, op.cit.

Using Eqs 2, 10 and 11 and letting $\mu = \mu_0$ gives:

$$\frac{L_w}{L_A} = \frac{R_w}{|Z_A|} = \frac{\frac{1}{r_o} + \frac{1}{r_i}}{\sqrt{2 \sigma_w \omega \mu_0} \log_e (r_o/r_i)}$$

Using the dimensions of Fig. 1, a frequency of 50 Mc/s, and the conductivity of silver, 6.2×10^7 mhos/meter.

$$\frac{R_w}{|Z_A|} \approx 0.07 \%$$

Clearly, wall resistance and internal inductance are negligible.

2.5 Accuracy

The greatest error is in treating the taper section as a constant impedance transmission line. We use the dimensions of Fig. 1 which is admittedly a poor design for this approximation. This will give an extremum in error.

$$k = 2.04 \quad x_o = 0.2 \text{ inches} \quad x_i = 0.17 \text{ inches}$$

Using Eq 7, $\omega L_T = 6.32$ ohms at 500 Mc/s and the error is 0.66 ohms, a 9.5% error. This is a serious error, but it is negligible if one makes difference impedance measurements as will be demonstrated later. It is interesting to compute the resulting error in Z_3 . For this calculation the maximum percentage error will occur at the lowest value of Z_1 , namely $Z_1 = Z_A$ (Eq 2). At 500 Mc/s, $Z_A \cong j 4.5$ ohms. $Z_2 = j \omega L_T + Z_A = j 10.82$ ohms if we use Eq 7 and $Z_2 = j 11.48$ ohms if we use only the first term in Eq. 7. Using Eq 9 the two values of Z_3 obtained are $j 65.0$ and $j 66.7$ respectively, a 2.6% difference.

This is roughly the per cent error one expects in the impedance measuring apparatus. Therefore, our approximation roughly doubles the possible error.

An additional, but small error is introduced by treating section one as a lumped impedance. The percentage error in Z_A is:

$$\frac{\beta l_1 - \tan \beta l_1}{\tan \beta l_1} \cong 0.2\% \quad \text{at } 500 \text{ Mc/s and } \mu = \mu_0.$$

3. DESIGN

One can alter the length l_1 , l_2 , and l_3 in Fig. 1 to obtain a better design. The dimensions of section one should be adjusted such that the ferrite ring will occupy a large portion of volume and still accomodate the range of ring sizes desired. In order to maintain negligible shunting capacitance between the faces of the toroid, l_3 must not be decreased too much. This requirement is met if the capacitive reactance $\frac{1}{\omega C} = \frac{l_1}{\omega \epsilon' \pi r_0^2}$ is very much less than ωL_1 . Here $\frac{1}{\epsilon'} = \frac{1}{\epsilon_0} + \frac{l_f}{l_1} \left[\frac{1}{\text{Re}(\epsilon)} - \frac{1}{\epsilon_0} \right]$ where ϵ is the dielectric constant of the ferrite ring.

A taper much shorter than a quarter wavelength in length is equivalent to an abrupt or discontinuous change in the inner and outer radii. Since the greatest error is introduced in the taper section, one should hold the length of this section to a minimum. However, one must be careful that at no point along the taper section does the ratio $\frac{r_0}{r_i}$ decrease enough to produce an appreciable shunting capacitance. $C = \frac{2\pi\epsilon_0}{\log_e(r_0/r_i)}$ farads/meter for a constant impedance line. This capacitive reactance must be less by orders of magnitude than the series inductive reactance of

$$\frac{\omega\mu_0}{2\pi} \log_e \frac{r_0}{r_i} \quad \text{henrys/m}$$

Finally, it is desirable to maintain l_3 as small as possible as this simplifies Eq 9. Also, the smaller l_3 , the less the impedance Z_1 is isolated from the point of impedance measurement. This means that the error in Z_1 due to an error in measuring Z_3 is decreased as l_3 is decreased. This is important because as computed earlier a 2.6% error in Z_3 corresponded to a 9.5% error in Z_2 for a large l_3 .

Figure 2 shows a better design. The major fault with this design is the small r_i in Section One. However, a steeper taper in the inner conductor might have introduced appreciable capacitive shunting.

4. MEASUREMENTS

4.1 Impedance Measuring Apparatus

The impedance measurements may be accomplished by any of several methods:⁶

1. Standing-wave ratio measurements with a slotted line
2. Byrne Bridge method
3. Admittance Comparator method
4. Directional-coupler methods
5. Probe methods
6. Hybrid Junction methods

Methods 1, 2, and 3 are available commercially. We chose the Byrne Bridge method and purchased the Hewlett-Packard VHF Bridge which allows a

⁶ These methods are discussed in Section 4-10 of Electronic Measurements, Terman, F.E. and Pettit, J.M., McGraw-Hill Book Co., 1952, pp 157-165

coverage from 50 Mc/s to 500 Mc/s. A H. P. signal generator and a H. P. detector were used in conjunction with the bridge.

4.2 Measurements with the Three Coaxial Inductors

Figure 3 shows a third coaxial inductor. Each of the three inductors have different dimensions. Measurements were made on two ferrite rings with each of the inductors. Figures 4 and 5 show the resulting curves of μ_1 and μ_2 . Inductors No. 2 and No. 3 give identical readings. Inductor No. 1 in Fig. 1, being of the poorest design, gives values a little different from those obtained with the other inductors. However, as noted earlier for inductor No. 1, a small error in the Z_1 measurement corresponds to a higher error in Z_3 and, therefore, a high error in μ_1 and μ_2 . Obtaining essentially the same values of μ_1 and μ_2 with the three different geometries serves as a partial verification of the foregoing analysis.

4.3 Calibration

One must determine $l_2 + l_3$ for use in the modified form of Eq 9. To do this, one inserts in section one a brass toroid of dimensions r_o , r_i and l_1 . The measurements made are $Z_B = j Z_o \tan \beta(l_2 + l_3)$. The lowest curve in Fig. 6 shows the value of $l_2 + l_3$ versus frequency for inductor No. 2. The curve shows roughly a 1% increase over the frequency range which seems to be typical of measurements with our bridge. All of the points deviate within experimental error from a straight line.

Rather than compute by Eq 2 the value of Z_A , it is measured by removing the brass shorting ring and making impedance measurements. Solving the modified form of Eq 9 for Z_A gives:

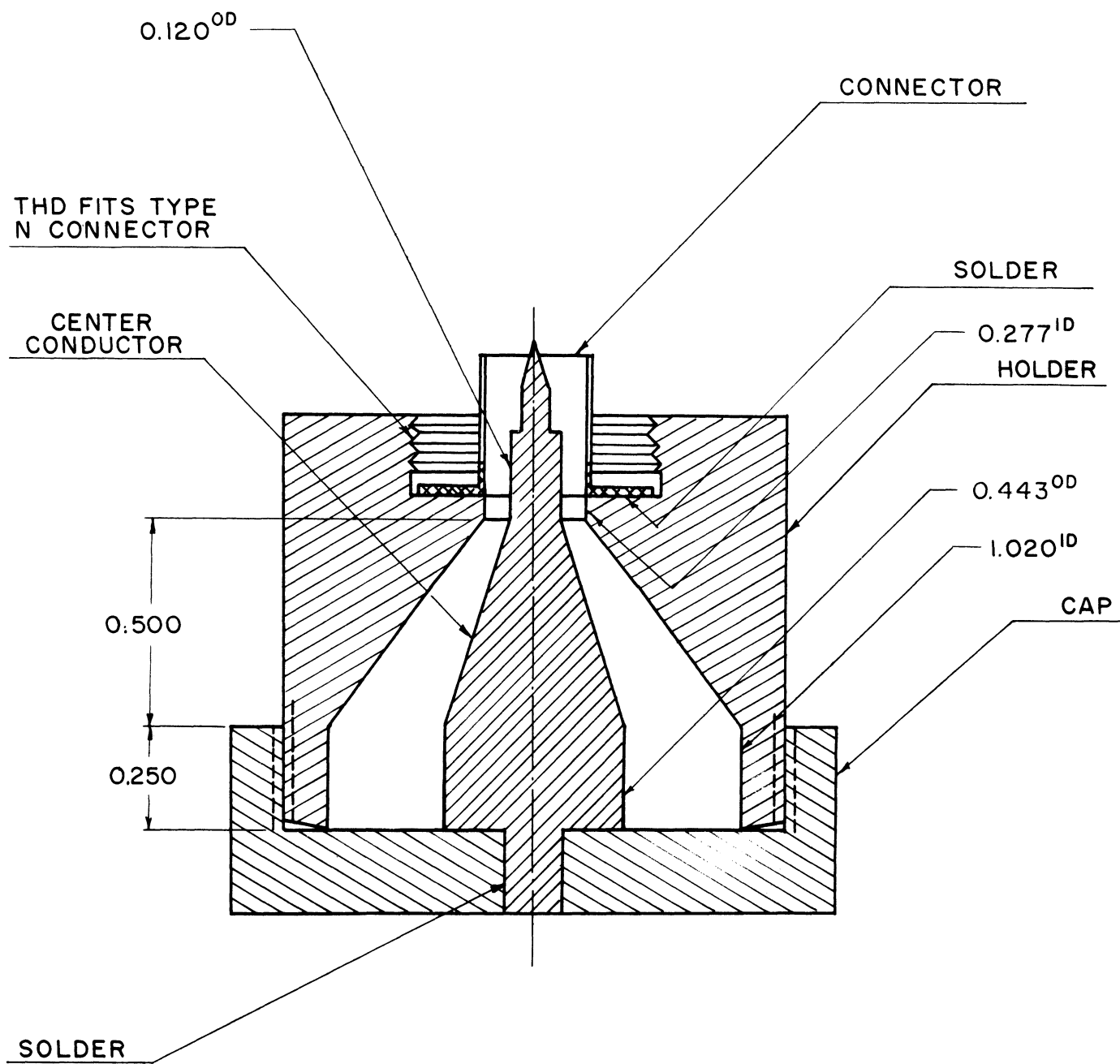


FIG 3

ASSEMBLY, COAXIAL INDUCTOR NO 3
DIMENSIONS IN INCHES

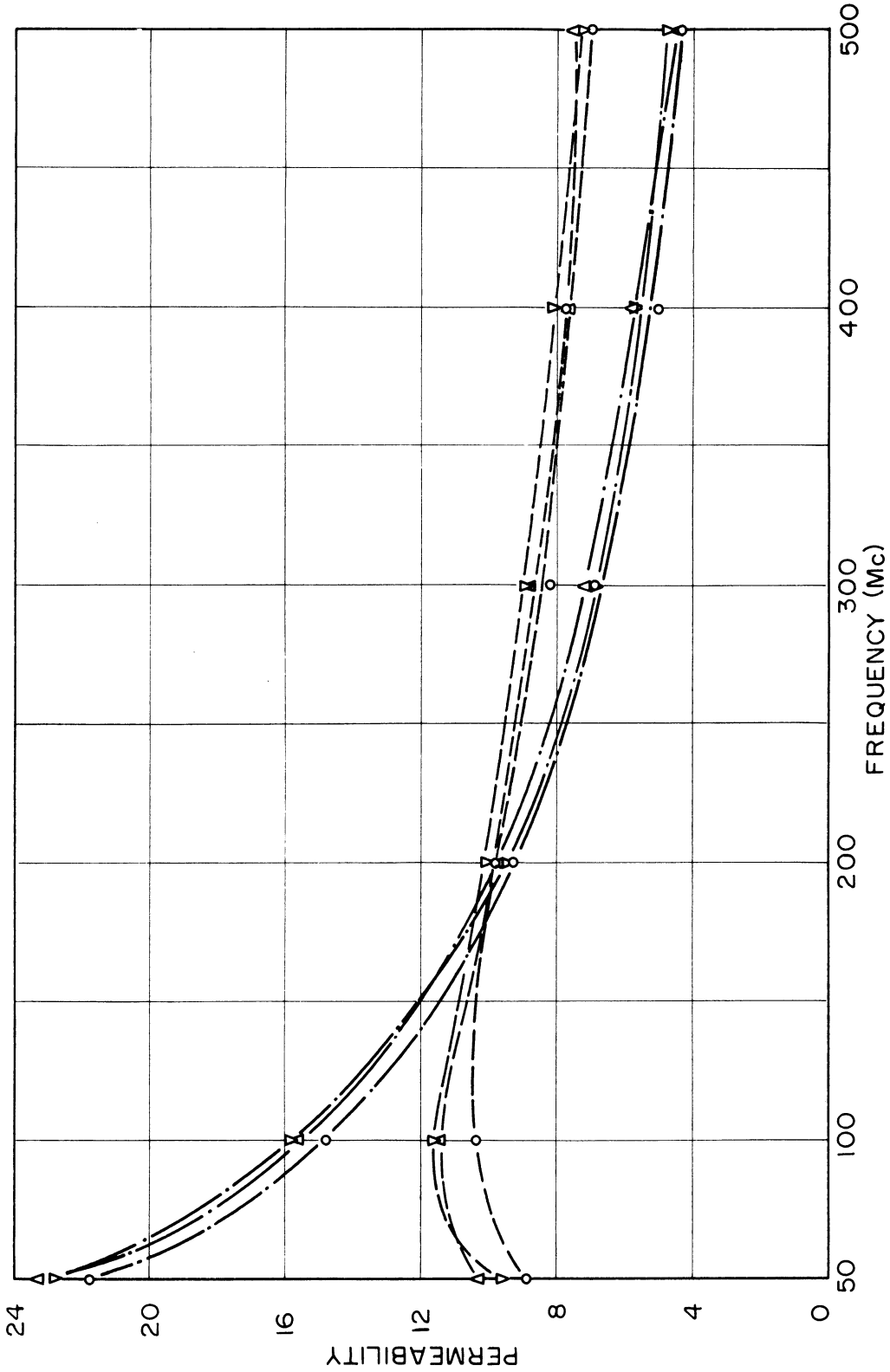


FIG 4
 μ_1 & μ_2 MEASURED BY DIFFERENT INDUCTORS
COAX IND #1
COAX IND #2
COAX IND #3
CORE A-61-1

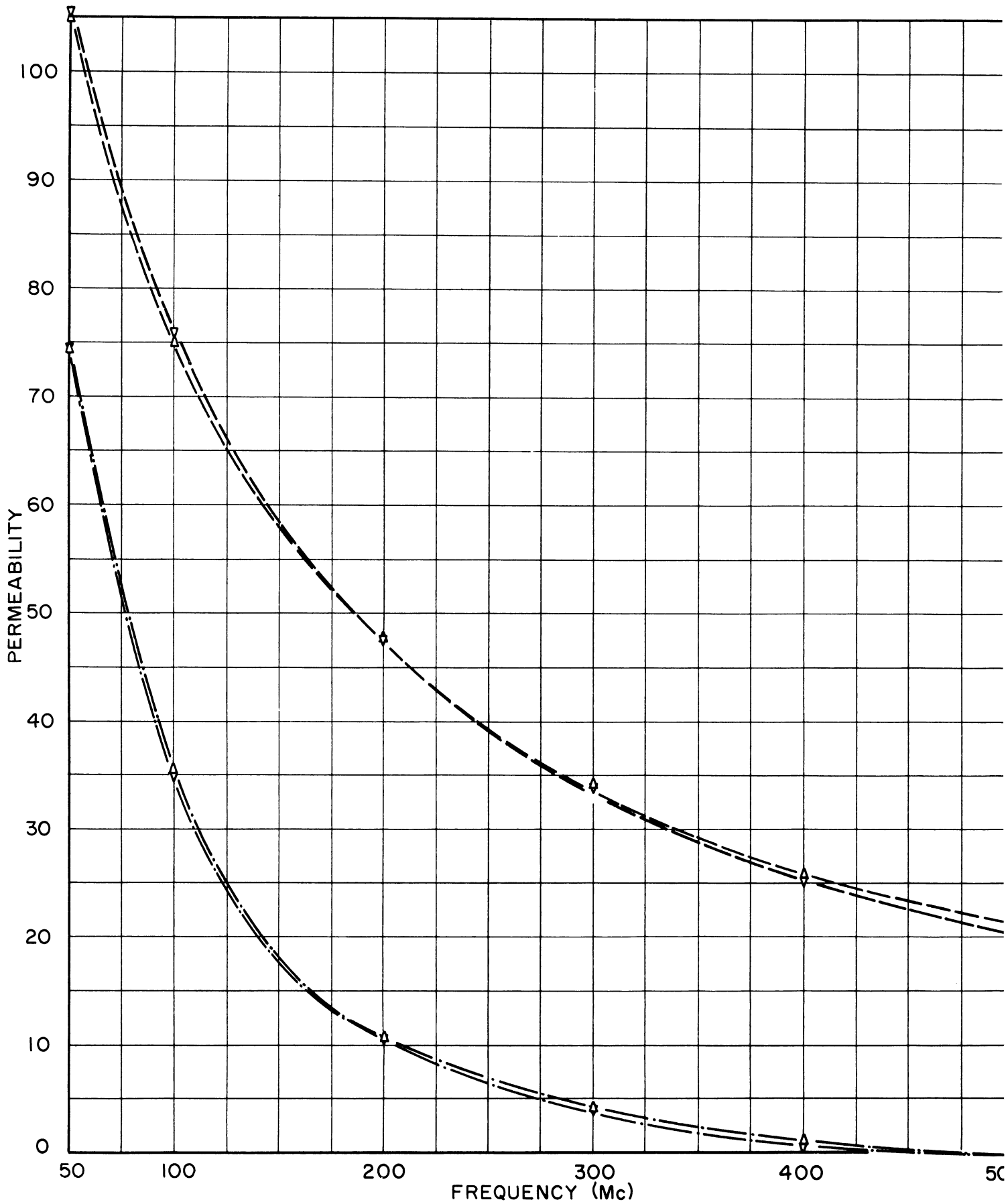


FIG 5
 μ_1 & μ_2 MEASURED BY DIFFERENT INDUCTORS

Δ COAX IND #2
 ∇ COAX IND #3
 — · — μ_1
 - - - μ_2

CORE A-127-1

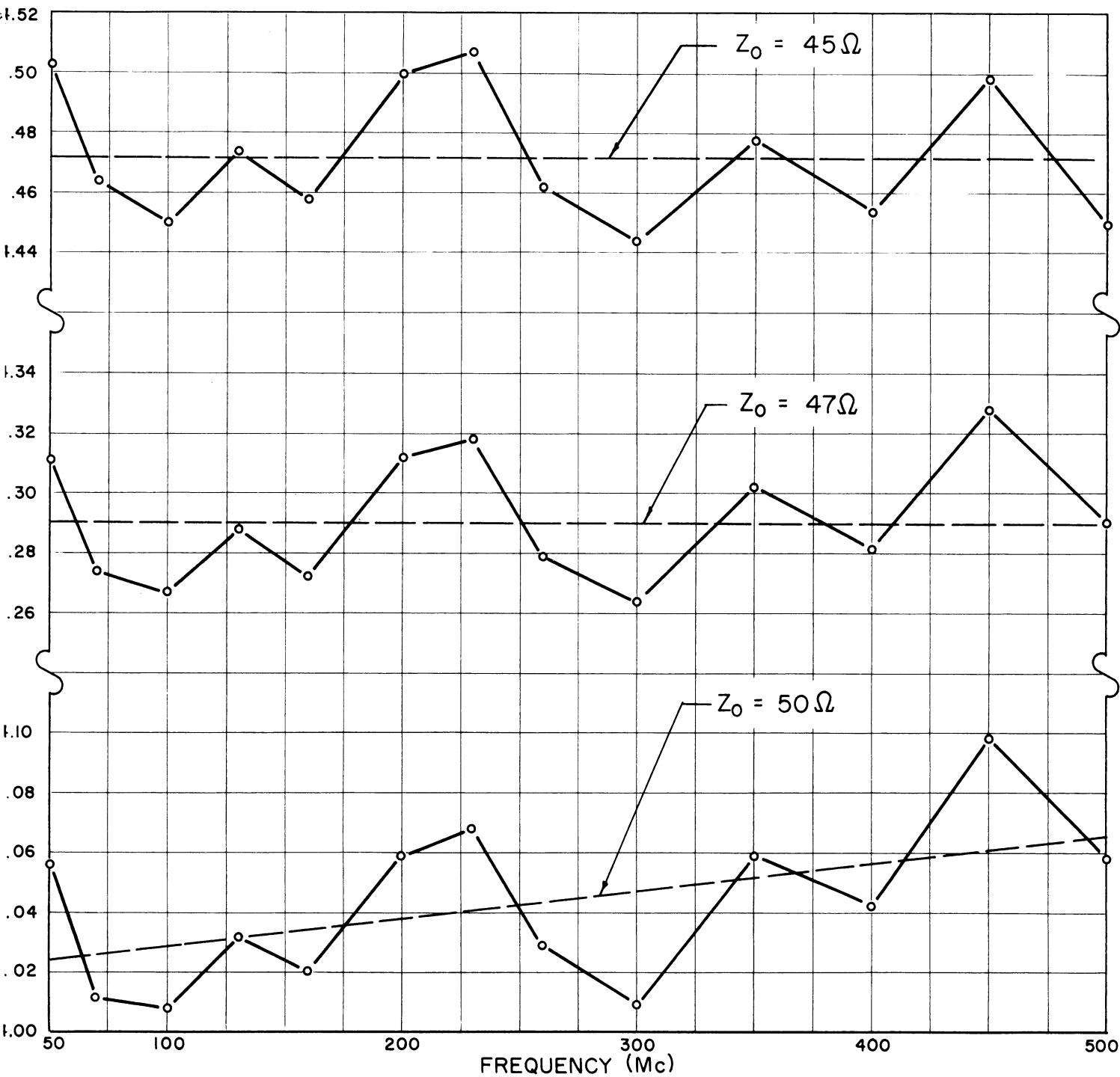


FIG 6
 CALIBRATION CURVES: $l_2 + l_3$ VS $\frac{\omega}{2\pi}$

$$Z_A = Z_0 \frac{Z_3 - jZ_0 \tan \beta(l_2 + l_3)}{Z_0 - jZ_3 \tan \beta(l_2 + l_3)} = \frac{Z_3 - Z_B}{\frac{1}{Z_0^2}(Z_0^2 - Z_3 Z_B)} \quad (12)$$

The lowest curve in Fig. 7 shows $\frac{Z_A}{\omega/\omega_0}$ versus frequency where $\frac{\omega_0}{2\pi} = 100$ Mc/s. This curve shows a 10% increase over the frequency range. Deviations from a straight line are again within experimental error. The average value of $\frac{Z_A}{\omega/\omega_0}$ gives an inductance L_A that is about 10% below the theoretical value. The value of L_A was 9% below the theoretical value for both of the other inductors.

The errors indicated by these calibration curves are not serious because we use the values actually measured for computing μ_1 and μ_2 . We believe that they are inherent in the bridge. Since repeated measurements give the same curves it is reasonable to use the values actually measured. Then only the change in impedance is used in calculating μ_1 and μ_2 .

On inductor No. 2 the calibration measurements were made twice; once with the shorting ring as described above and once with the short in effect placed closer to the point of impedance measurement. The latter method resulted in an average value of $l_2 + l_3$ of 3.50 cm instead of 4.03 cm and an average value of $\frac{Z_A}{\omega/\omega_0}$ of 1.39 instead of 0.833 ohms. Ferrite rings gave identical μ_1 and μ_2 curves versus frequency regardless of which calibration was used. This indicates that the values of calibration data themselves are not important so long as difference measurements are used in calculating μ_1 and μ_2 .

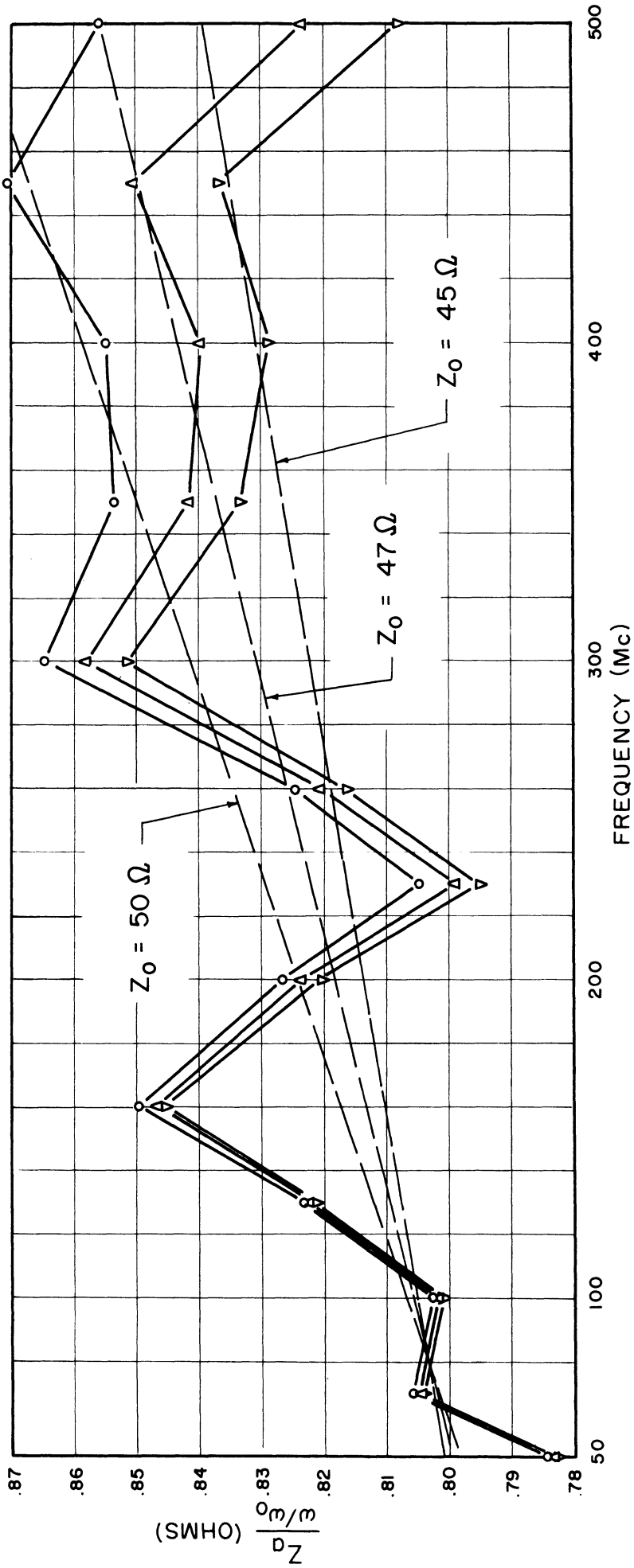


FIG 7
 CALIBRATION CURVES: $\frac{Z_D}{\omega/\omega_0}$ VS $\frac{\omega}{2\pi}$
 FOR DIFFERENT VALUES OF Z_0

4.4 The Value of Characteristic Impedance, Z_0

Figure 8 shows a cross-section of the transmission line of length l_3 . It is not a simple straight pipe. The ratio $\frac{r_0}{r_1}$ varies along the length of the line, all of which is not visible. Values of characteristic impedance for that part of the line, which is visible have been calculated and an average value of 46 ohms has been obtained. The manufacturer quotes a value of 50 ohms for his bridge and the latter value has been used. However, if one uses slightly lower values the curves of $l_2 + l_3$ and $\frac{Z_A}{\omega/\omega_0}$ are affected in a favorable manner. Figures 6 and 7 show curves for which the values of characteristic impedance used were 45 and 47 ohms. The result is to decrease the positive slope of these curves. In Fig. 6 the slope is zero. In Fig. 7 the increase over the frequency range is 7.5% for $Z_0 = 47$ ohms and 5% for $Z_0 = 45$ ohms. The effect of using $Z_0 = 46$ ohms on the μ -curves is negligible as Fig. 9 shows.

4.5 Procedure

Once the calibration is made, a ferrite ring is placed in the inductor and Z_3 is measured. Z_1 is then calculated using Eq 12. Then μ_1 and μ_2 are calculated using the following equations which are derived from Eq 5:

$$\mu_1 - 1 = \frac{k [\text{Im}(Z_1) - |Z_A|]}{l_f \omega / \omega_0} \tag{13}$$

$$\mu_2 = \frac{k \text{Re}(Z_1)}{l_f \omega / \omega_0} \tag{14}$$

where $k = \frac{2 \pi}{\omega_0 \mu_0 \log_e \frac{r_2}{r_1}}$ = a constant since for our cores $\frac{r_2}{r_1}$ is a constant.

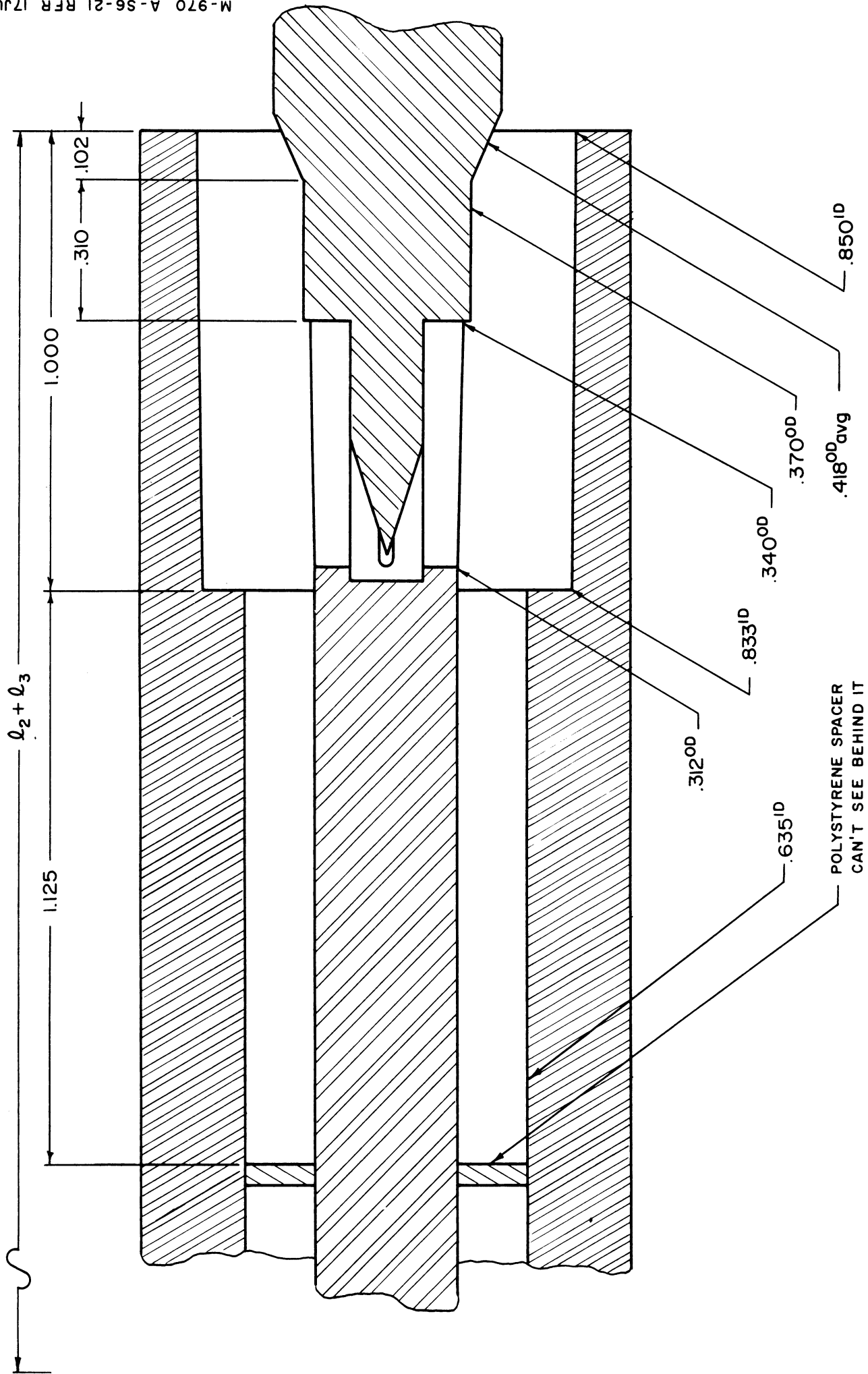


FIG 8
SECTIONS II & III OF COAXIAL INDUCTOR #2: THE TRANSMISSION LINE
(DIMENSIONS IN CENTIMETERS)

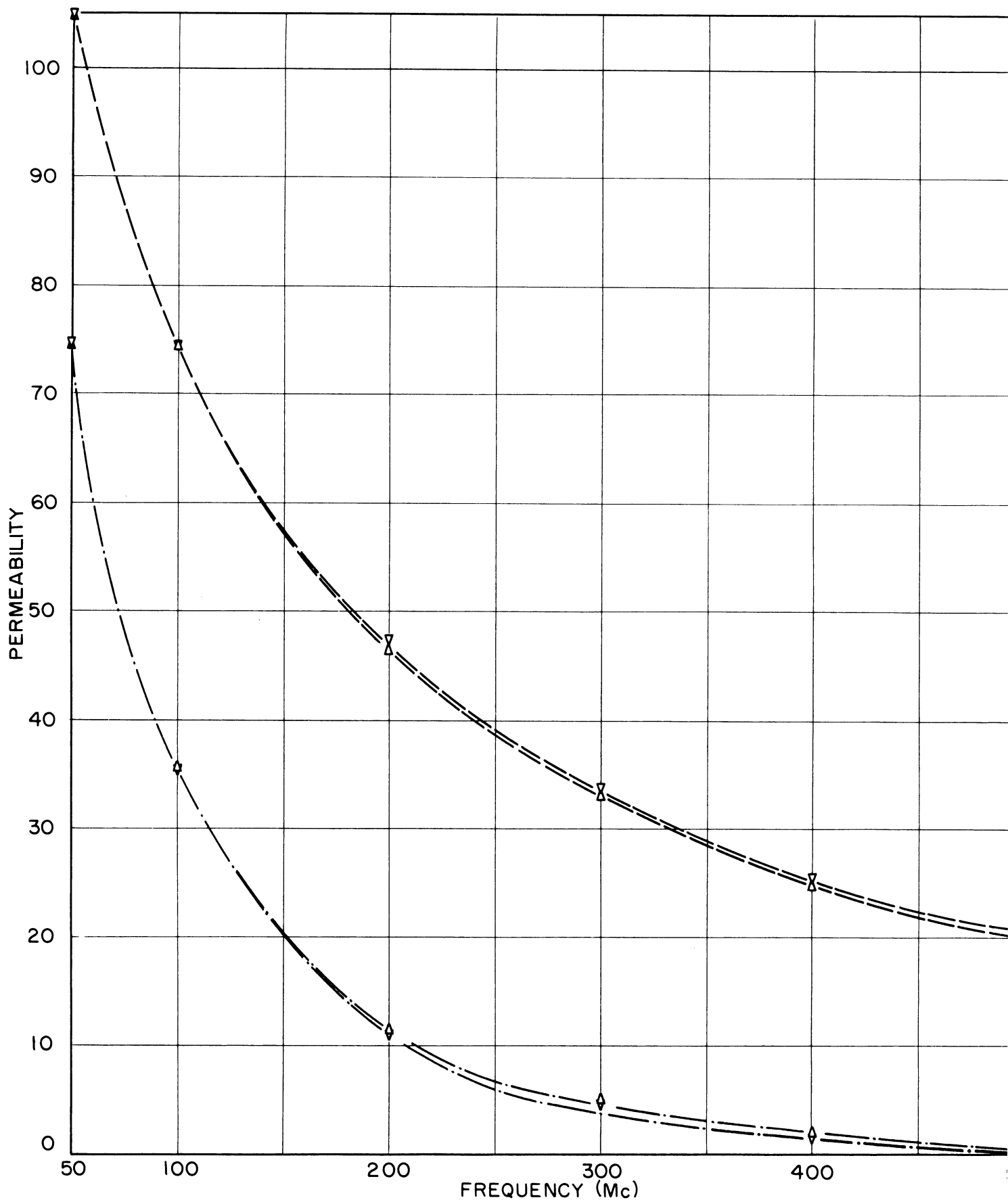


FIG 9

μ CURVES USING TWO DIFFERENT VALUES OF Z_0

Δ $Z_0 = 46 \Omega$

∇ $Z_0 = 50 \Omega$

--- μ_1

-.-.- μ_2

COAX. IND. #2, CORE NO A-61-1

4.6 Z-θ Chart

The use of Eq 12 may be avoided by use of the Z-θ chart.⁷ Then the calibration procedure must include the computation of $\frac{l_2 + l_3}{\lambda}$. We computed and drew up a Z-θ chart of 12" radius. It was found satisfactory at the higher frequencies and over the entire frequency range for cores of high permeability. For the lower frequencies data on low permeability cores could not be used on the chart because of the difficulty in reading the phase angle accurately on the chart for low values of Z₁.

4.7 P-Contours

Since the calculation of μ₁ and μ₂ is tedious even using the Z-θ chart, P-contours were compiled which greatly speeded the calculations. Computations, heretofore not mentioned, are corrections of the bridge's readings according to the calibration curves of a and b supplied by the manufacturers. These computations are:

$$Z_3 \text{ corrected} = Z_3 \text{ measured} (1 + a) \tag{15}$$

$$\theta_3 \text{ corrected} = \frac{\omega}{\omega_0} \theta_3 \text{ measured} + b \tag{16}$$

These corrections plus Eqs 12, 13 and 14 are all included in calculating the P-contours. Let us define

$$P_1 = l_f(\mu_1 - 1); \quad P_2 = l_f \mu_2$$

Then from Eqs 12, 13 and 14:

⁷ Pages 152-157 of Ramo and Whinnery, op.cit.

$$Z_3 \sin \theta_3 = \frac{P_1 \omega / k \omega_0 + Z_A + Z_B}{1 - \frac{Z_B}{Z_0^2} [P_1 \omega / k \omega_0 + Z_A - P_2 \omega / k \omega_0 \cot \theta_3]} \quad (17)$$

and

$$Z_3 \cos \theta_3 = \frac{P_2 \omega / k}{1 - \frac{Z_B}{Z_0^2} [P_1 \omega / k \omega_0 + Z_A + P_2 \omega / k \omega_0 \tan \theta_3]} \quad (18)$$

In Eqs 17 and 18 all values of Z are absolute values. θ_3 is the phase angle of Z_3 .

These implicit relations allow the calculation of Z_3 and θ_3 corresponding to a given set of values of P_1 and P_2 . The procedure is:

1. Choose a value for P_1 and a value for P_2
2. Guess a value for θ_3
3. Calculate the right-hand sides of Eqs 17 and 18
4. Take the ratio of these two computations and equate to $\tan \theta_3$.
Thereby determine θ_3 .
5. Compare this value of θ_3 with the value guessed earlier. If they are not equal, use the computed value as a more intelligent guess and repeat the computation until the computed value of θ_3 equals the guessed value.
6. Calculate Z_3 from left side of either Eq 17 or 18.

The values of Z_3 and θ_3 just calculated refer to the corrected values. So one must use Eqs 15 and 16 to find the measured values. The P-contours thus calculated are plotted in the Z_3 measured - θ_3 measured - plane. P-contours must be calculated at each frequency of interest. Figure 10 shows P-contours for a frequency of 200 Mc/s. Roughly 60 computations are necessary to establish this chart. But it will be used for hundreds of measurements. In addition,

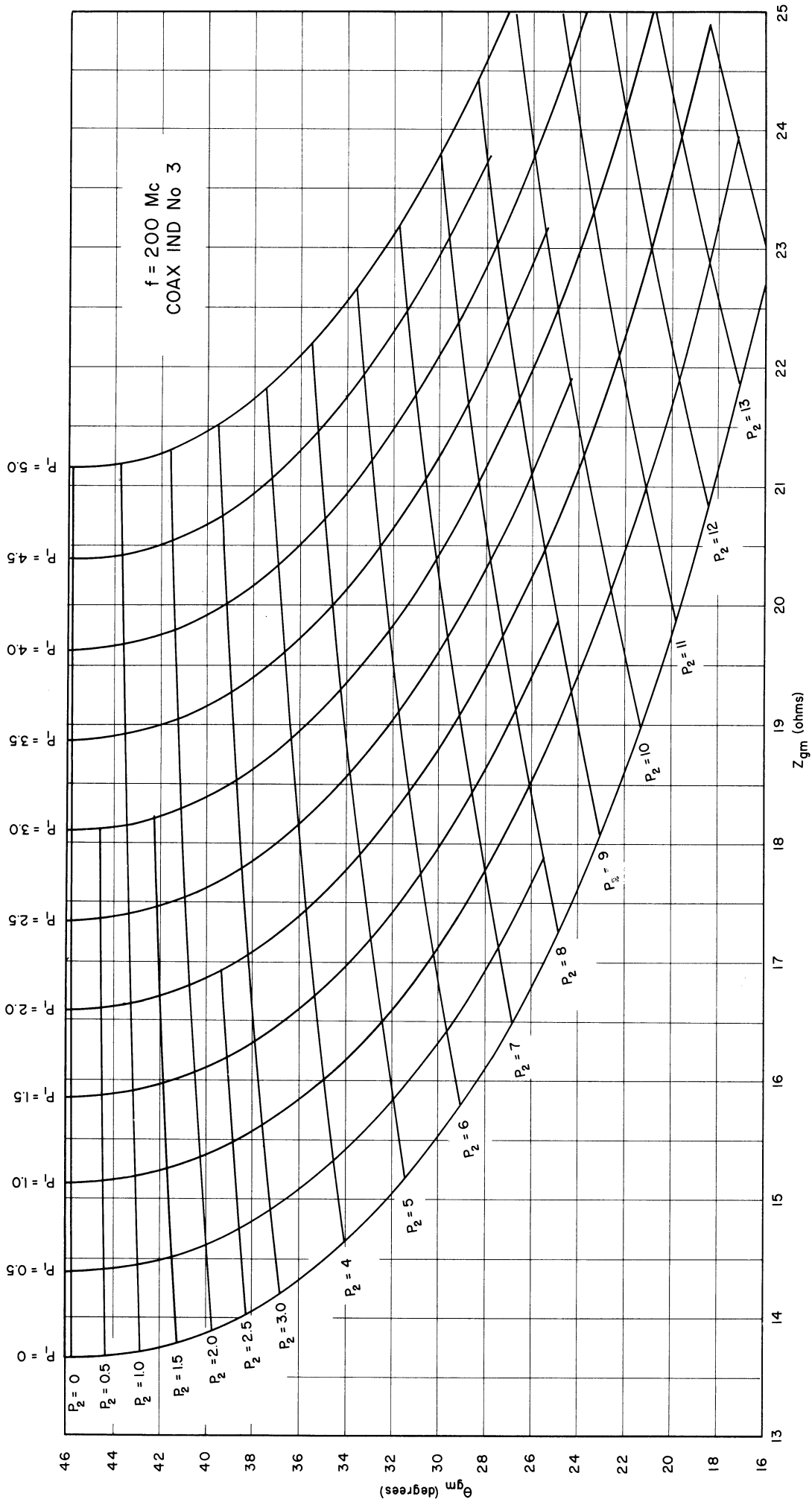


FIG 10
P CONTOURS

computational errors are quickly isolated in computing the chart, whereas corresponding errors made in evaluating the data for each core according to the procedure of paragraph 4.5 would be extremely difficult to isolate. We have calculated P-contours for frequencies of 50, 100, 200 and 500 Mc/s.

One merely takes the measured values of Z_3 and θ_3 to the P-contours and reads the values of P_1 and P_2 . Dividing by l_f gives $\mu_1 - 1$ and μ_2 respectively. Thus $\mu_1 - 1$ and μ_2 are now easily computed.

5. CONCLUSION

The coaxial inductor permits the rapid measurement of μ_1 and μ_2 of a large number of ferrite toroids over a frequency range of 50 to 500 Mc/s. A wider range is permitted if one has the necessary impedance measuring apparatus. The measurements are accurate to perhaps 5% if the inductor is judiciously designed and the impedance measuring apparatus is sufficiently accurate. The technique of measurement is rapid because an initial balance is not necessary and because the ferrite ring does not require a snug fit in the inductor. The only requirement is that it fit concentrically. We accomplish this by sticking the ring in place with vacuum grease which does not affect the measurements. The inductor packed with vacuum grease had the same impedance as the air filled inductor. Finally, the use of P-contours makes the computations very rapid and there is little source of error.

ACKNOWLEDGEMENTS

The author wishes to acknowledge the counsel of members of the Department of Electrical Engineering of the University of Michigan. In particular the encouragement and counsel of Mr. D. M. Grimes has been most helpful.

DISTRIBUTION LIST

1 copy Director, Electronic Research Laboratory
Stanford University
Stanford, California
Attn: Dean Fred Terman

1 copy Commanding Officer
Signal Corps Electronic Warfare Center
Fort Monmouth, New Jersey

1 copy Chief, Engineering and Technical Division
Department of the Army
Washington 25, D.C.
Attn: SIGJM

1 copy Chief, Plans and Operations Division
Office of the Chief Signal Officer
Washington 25, D.C.
Attn: SIGOP-5

1 copy Countermeasures Laboratory
Gilfillan Brothers, Inc.
1815 Venice Blvd.
Los Angeles 6, California

1 copy Commanding Officer
White Sands Signal Corps Agency
White Sands Proving Grounds
Las Cruces, New Mexico
Attn: SIGWS-CM

1 copy Commanding Officer
Signal Corps Electronics Research Unit
9560th SU
Mountain View, California

1 copy Mr. Peter Haas
High Frequency Standard Section
Central Radio Propagation Laboratory
National Bureau of Standards
Washington 25, D.C.



3 9015 03483 1670

| | |
|-----------|---|
| 75 copies | <p>Transportation Officer, SCEL Evans Signal Laboratory Building No. 42 Belmar, New Jersey</p> <p>For - Signal Property Officer Inspect at Destination File No. 25052-PH-51-91(1443)</p> |
| 1 copy | <p>H. W. Welch, Jr. Engineering Research Institute University of Michigan Ann Arbor, Michigan</p> |
| 1 copy | <p>Document Room Willow Run Research Center University of Michigan Willow Run, Michigan</p> |
| 14 copies | <p>Electronic Defense Group Project File University of Michigan Ann Arbor, Michigan</p> |
| 1 copy | <p>Engineering Research Institute Project File University of Michigan Ann Arbor, Michigan</p> |
| 1 copy | <p>Dr. J. K. Galt Bell Telephone Laboratories, Inc. Murray Hill, New Jersey</p> |
| 1 copy | <p>Dr. G. T. Rado Naval Research Laboratory Washington 25, D.C.</p> |
| 1 copy | <p>Dr. R. M. Bozorth Bell Telephone Laboratories, Inc. Murray Hill, New Jersey</p> |